Irradiation Effects in Space Solar Cells Made of Multiple Absorbers

M.J. Romero, R.J. Walters,[1] M.M. Al-Jassim, S.R. Messenger,[1] and G.P. Summers[1]
National Renewable Energy Laboratory (NREL), 1617 Cole Boulevard, Golden, CO 80401-3393
Phone: 303-384-6653, Fax: 303-384-6604, Email: mromero@nrel.gov
[1]Naval Research Laboratory (NRL), Code 6615, 4555 Overlook Ave., S.W., Washington DC 20375

ABSTRACT

Solar cells made of multiple absorbers are a commonly used approach for improving efficiency due to their extended range of spectral sensitivity. Indeed, efficiencies nearing the theoretical maximum have been achieved with a triple-junction device made of $In_{0.51}Ga_{0.49}P$ ($InGaP_2$), GaAs, and Ge solar cells connected in series. For extraterrestrial applications, there is the added requirement of radiation tolerance. The main challenge for space power-generation is therefore the development of highly efficient and radiation-tolerant devices. We have investigated several aspects of the radiation response of solar cells made of multiple absorbers, such as multijunction devices and quantum-well solar cells. Novel possibilities such as quantum-dot solar cells and ordered-disordered heterostructures are proposed.

INTRODUCTION

Future satellite systems are projected to fly in orbit in or near the proton radiation belts, which extend from 2,000 to 10,000 km of altitude (MEO: Medium-Earth Orbit). Radiation effects can be very severe in these orbits, and high-efficiency solar cells with minimal degradation under cosmic particle bombardment are required.

Recent attempts to boost efficiencies are based on extending the spectral sensitivity by the use of multiple absorbers. Multijunction solar cells hold the promise of increasing the maximum attainable conversion efficiency well above the Shockley and Queisser (SQ) limit [1]. Indeed, the maximum practical efficiency for a solar cell (of 32.2% at 1-sun, AM1.5) has been achieved with a triple-junction device made of $In_{0.51}Ga_{0.49}P$ ($InGaP_2$), GaAs, and Ge solar cells connected in series. Quadruple-junction devices are being developed, and the search for 1-eV absorbers to add a junction to the InGaP/GaAs/Ge cell is being conducted at NREL [2].

Other efforts have been made to improve solar cell efficiencies by the use of quantum wells as an intermediate level that absorbs additional lower-energy photons [3]. One question is whether quantum-well solar cells have their efficiency restricted by the SQ limit. Quantum-well solar cells have the potential to increase the maximum attainable conversion efficiency above the limit of conventional solar cells by extracting hot carriers to produce either higher photovoltages or photocurrents. However, if phonon-assisted relaxation of hot carriers is not prevented, a quantum-well solar cell ideally behaves as a single-junction solar cell.

The use of these advanced devices for space power-generation is limited by their radiation resistance. We have investigated several aspects of the radiation response of these solar cells by beam injection methods. In multijunction devices, some of the critical issues are the occurrence of a radiation-induced sublattice order-disorder transition in $InGaP_2$ [4], interconnecting junctions, type conversion under irradiation, and buffer-layer engineering when needed. In quantum-well solar cells, some of the matters to address are interdiffusion between the wells and the barriers and how carrier excess transport is influenced by irradiation.

We critically review these solar cells and explore novel schemes for high efficiency solar cells with improved radiation resistance.

MULTIJUNCTION SOLAR CELLS

Monolithic multijunction (MJ) solar cells consist of several single cells of different spectral sensitivity connected in series. Under irradiation with high-energy electrons and protons, as occurs in space, all junctions are degraded simultaneously. The most vulnerable junction determines the radiation response of the entire cell because the individual cells are series connected. For the lattice-matched $InGaP_2/GaAs$ tandem, $InGaP_2$ has shown much higher radiation tolerance than GaAs; therefore, the radiation response of the tandem is limited by the radiation response of the GaAs sub-junction cell. At end of life, the effects of subsequent irradiation might nullify the higher power density gained from the tandem. Because the design of the multijunction devices requires matching the current density of each individual solar cell to the solar spectra irradiance, this requirement should be satisfied throughout the life of the solar cell in space. Therefore, damage coefficients under electron and proton irradiation for each individual cell should be matched as closely as possible for their use in space. In light of this, we have investigated possibilities other than the conventional $InGaP_2/GaAs$.

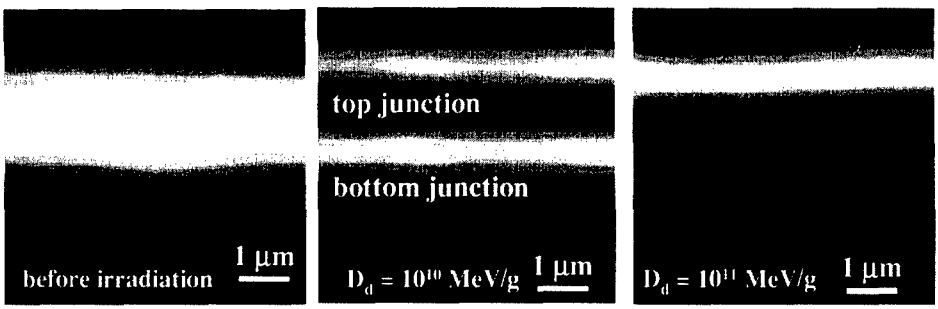

Figure 1. Cross-sectional EBIC images of the mismatched tandem cell ($In_{0.65}Ga_{0.35}P/In_{0.17}Ga_{0.83}As$) at different displacement damage doses, D_d.

Non-lattice-matched multijunction solar cells

The high-efficiency, commercially available leading technologies are the dual-junction $InGaP_2/GaAs$ and triple-junction $InGaP_2/GaAs/Ge$ solar cells. The challenge of these technologies is to lattice match the different semiconductors at their interfaces to prevent the generation of threading dislocations. However, $InGaP_2$ and GaAs are not the optimum semiconductors for the solar spectrum in space (AM0). This tandem has no degree of freedom to suit the spectral irradiance, whereas this is not the case for $In_xGa_{1-x}P$ and $In_yGa_{1-y}As$, where the indium content might be optimized for spectral sensitivity. Buffer engineering should then be applied to accommodate the lattice mismatch. Several dual-junction (DJ) cells have been investigated. One of them is the conventional DJ $InGaP_2/GaAs$ of *n-p* polarity commercialized by Spectrolab. To explore other systems, $In_{0.49}Ga_{0.51}P/In_{0.03}Ga_{0.97}As$ (nearly lattice-matched) and $In_{0.65}Ga_{0.35}P/In_{0.17}Ga_{0.83}As$ (lattice mismatched) DJ devices of *n-p* polarity were fabricated on

GaAs substrates by metal-organic vapor-phase epitaxy (MOVPE) [5]. Linearly graded buffer layers of InGaAs have been used here, which is a better approach to progressively relax the strain [6,7] over step-graded or single layers. In this way, InGaAs epilayers of high quality have been achieved. Testing their radiation response is of interest for their use in space. The devices were irradiated with protons in the MeV energy range.

Figure 1 shows cross-sectional electron-beam-induced-current (EBIC) images of the mismatched tandem cell at different displacement damage doses, D_d [8]. Before irradiation, the subcells are not resolved due to the diffusion length at the base of the top cell being much longer than the base thickness. After irradiation, by the degradation of the diffusion length, both the top and bottom junctions are finally resolved. From these images, it is apparent that the bottom cell is more susceptible to irradiation than the top cell. Diffusion lengths (L) are subsequently estimated by EBIC, and the diffusion-length damage coefficient, κ_L (g cm^{-2} MeV^{-1}) is evaluated from fits to the diffusion-length degradation equation [9]:

$$\frac{1}{L^2(D_d)} = \frac{1}{L_0^2} + \kappa_L D_d , \qquad (1)$$

where L_0 is the diffusion length prior to irradiation. The values thus determined for κ_L for the various semiconductor materials studied are given in Table I.

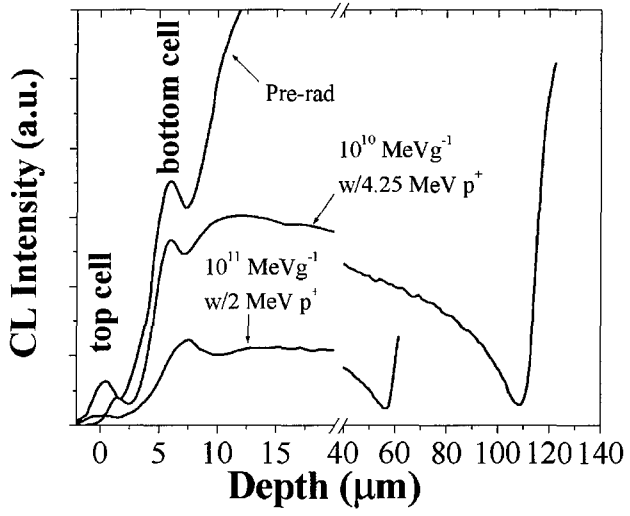

Figure 2. CL intensity measured as a function of depth into the $In_{0.49}Ga_{0.51}P/In_{0.03}Ga_{0.97}As$ cell at different damage doses (in MeVg^{-1}).

Panchromatic cathodoluminescence (CL) measured on cross-sections allows the emission from each individual junction to be resolved, as shown in Figure 2. The positive peaks in the data occur at the location of each junction. For the post-irradiation data, the large negative peaks

occurring deep into the sample are a result of the heavy damage produced when the incident protons slow-down and stop in the material. Thus, the location of the negative peaks corresponds to the range of the incident protons. The intensity of the CL is progressively degraded under proton bombardment as a result of lifetime degradation, as expressed by

$$\frac{I}{I_0} = \frac{1}{1+\tau_0 \kappa_\tau D_d}, \qquad (2)$$

where τ_0 and I_0 are the minority-carrier lifetime and the emitted intensity prior to irradiation, respectively, and κ_τ (g s^{-1} MeV^{-1}) is the lifetime damage coefficient. The fits from equations 1 and 2 yield the damage coefficients for L and τ for each semiconductor, as detailed in Table I.

Table I. Diffusion-length and lifetime damage coefficients under proton irradiation for different semiconductors. ‡ Lower limit for the diffusion length.

	$In_{0.65}Ga_{0.35}P$	$InGaP_2$	$In_{0.49}Ga_{0.51}P$	GaAs	$In_{0.03}Ga_{0.97}As$	$In_{0.17}Ga_{0.83}As$
Carrier density (cm^{-3})	*p*-type, 1.5×10^{17}	*n*-type, 1.5×10^{16}	*p*-type, 1.5×10^{17}	*p*-type, 8×10^{16}	*p*-type, 1.5×10^{17}	*p*-type, 1.5×10^{17}
L_0 (μm)	1.40‡	0.30	1.50‡	2.50	2.05	1.89
κ_L (g cm^{-2} MeV^{-1})	5×10^{-11}	1×10^{-10}	7×10^{-11}	8×10^{-9}	1×10^{-10}	3×10^{-11}
$\tau_0\kappa_\tau$ (g MeV^{-1})	6×10^{-13}	1×10^{-12}	5×10^{-12}	5×10^{-11}	4×10^{-11}	6×10^{-11}

The κ_L damage coefficient is particularly useful in describing the radiation response, but this parameter is known to be sensitive to polarity, carrier density, and L_0, making a detailed comparison amongst the samples based on this parameter difficult. Furthermore, because the top cells are relatively thin, they are nearly insensitive to diffusion length degradation. The lifetime damage coefficient, $\tau_0\kappa_\tau$, on the other hand, is not as sensitive to these other parameters, so it provides a better means for comparing radiation tolerance. $\tau_0\kappa_\tau$ falls into the 10^{-12} g MeV^{-1} range for $In_xGa_{1-x}P$ and is approximately 5×10^{-11} g MeV^{-1} for $In_yGa_{1-y}As$, suggesting greater radiation resistance in the $In_xGa_{1-x}P$ material. Also, the data suggest that the addition of indium to $In_xGa_{1-x}P$ improves the radiation response while the opposite is true for $In_yGa_{1-y}As$.

Figure 3a shows the low-temperature CL spectra of $In_{0.49}Ga_{0.51}P$ measured at different damage doses. Prior to irradiation, the spectra are characterized by the band-to-band emission (e,h) at 1.913 ± 0.002 eV and a free-to-band transition associated with Zn acceptors (e, Zn^0). After doses as high as 5×10^{10} MeV g^{-1}, there are no evident effects on the spectra. However, at 1×10^{11} MeV g^{-1}, the band-to-band emission peak shifts toward higher photon energies, and the recombination path related to Zn is progressively deactivated. The former effect has been successfully explained by an order-disorder transition, as we will discuss later. The role of Zn impurities has been previously investigated in InP [10], and a defect complex involving Zn after irradiation has been suggested. These results suggest that there may be a similar effect in InGaP.

The effects of proton irradiation on the CL spectra of $In_{0.65}Ga_{0.35}P$ are shown in Figure 3b. Prior to irradiation, the $In_{0.65}Ga_{0.35}P$ emission is centered at 1.728 eV. After moderate irradiation, the emission slightly shifts to lower photon energies, although the overall luminescence is not much degraded. Note that this semiconductor has shown a lifetime

degradation coefficient as low as 6×10^{-13} g MeV^{-1}. Increasing the dose does not cause the emission to shift further, but the intensity is degraded. There is no evidence of shifting in the room-temperature spectra (not shown).

To fully interpret these results, a more extensive investigation needs to be conducted. It is believed that compositional modulation might be responsible for this effect. The higher the In content, the better the radiation resistance. Degradation is then primarily located in the gallium-rich regions of wider bandgap. Hence, after irradiation, the main emission of photons is from the indium-rich regions and the overall intensity shifts to lower energies. The effect is not observable at room temperature, as diffusion lengths are longer than the range of compositional modulation.

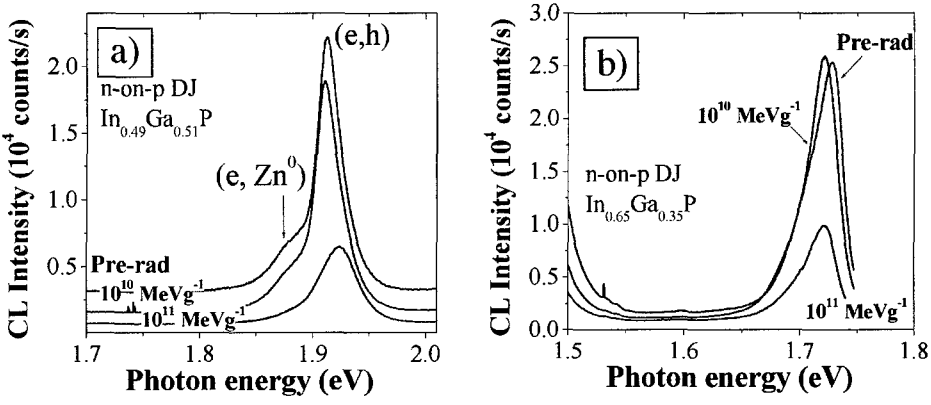

Figure 3. CL spectra measured at different damage doses (in $MeVg^{-1}$) for the $In_xGa_{1-x}P$ alloys (a) $In_{0.49}Ga_{0.51}P$, and (b) $In_{0.65}Ga_{0.35}P$.

The role of dislocations

Local observations by EBIC or CL indicate that dislocations act as efficient carrier recombination centers, representing a loss mechanism for photovoltaic conversion. For space solar cells, the question arises of how irradiation influences the electrical activity of dislocations. We have recently developed an EBIC method for defect recognition in each individual sub-cell of multijunction solar cells using filtered external illumination [11]. By means of this *light-biasing EBIC*, misfit dislocations are seen at the bottom cell of the $In_{0.65}Ga_{0.35}P/In_{0.17}Ga_{0.83}As$ tandem (Figure 4a), as well as dislocations threading through the top cell (Figure 4b). Under proton irradiation, the EBIC contrast of the misfit dislocations located at the bottom cell decreases, and the contrast for threading dislocations crossing the $In_{0.65}Ga_{0.35}P$ eventually vanishes.

In modeling the EBIC contrast, dislocations are assumed to be regions of a recombination lifetime, τ_D, different from that in the surrounding region, τ [12]. The mechanism governing the recombination at the defect site is not considered. Lifetimes are related to diffusion lengths through the diffusion coefficient $D = L_D^2/\tau_D = L^2/\tau$. The EBIC contrast is then defined by:

$$c = \Gamma \times F(L, z_D, E_b), \tag{3}$$

with Γ being the defect recombination activity and F a correction factor that groups geometric factors such as the depth of the defect z_D, the spatial distribution of the electron beam excitation, and the diffusion length L of the surrounding region. Therefore, measured contrast must be corrected by F to yield the defect recombination activity Γ. In a first-order approximation [12], Γ is given by:

$$\Gamma = \frac{\pi r_D^{\,2}}{D} \frac{1}{\tau_D} \tag{4}$$

where r_D is the effective radius of the defect. Thus, the reduction of the contrast under irradiation might be due to degradation of the diffusion length in the region surrounding the dislocation, instead of differences in the defect recombination activity. By simulation of the induced currents, we have confirmed that indeed *irradiation decreases the recombination activity of dislocations.*

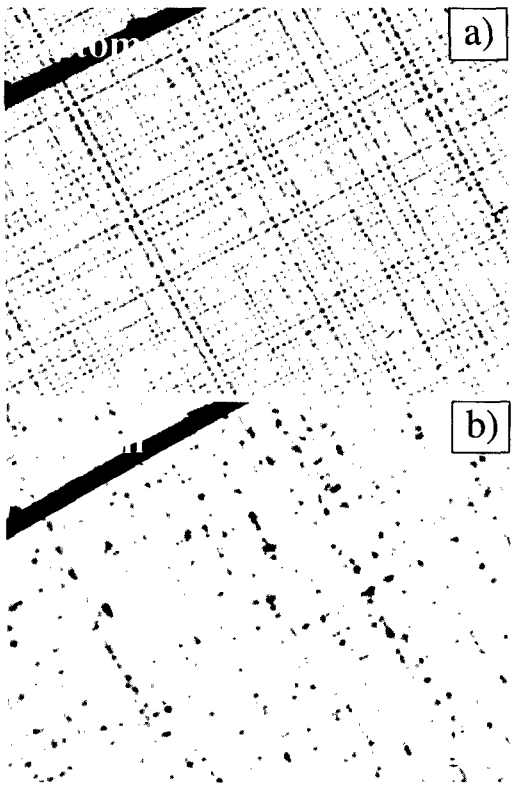

Figure 4. Defect imaging by EBIC: (a) misfit dislocations at the bottom cell, and (b) dislocations threading through the top cell of the lattice-mismatched $In_xGa_{1-x}P/In_yGa_{1-y}As$ structure.

Dislocations are one-dimensional disruptions of the lattice, which may be described in III-Vs by one-dimensionally distributed deep-levels and a space-charge region surrounding them. Defects induced by irradiation might either affect the density of active defect states at the dislocation or influence the surrounding space-charge region by carrier traps in the host semiconductor. Radiation effects on dislocations are considerably more in $In_xGa_{1-x}P$ than in $In_yGa_{1-y}As$.

Interconnecting junctions

Multijunction cell operation is allowed by interconnecting tunnel junctions, which are on the order of tens of nanometers in thickness. These nano-junctions connect the individual cells in series while minimizing absorption losses. High-energy electron and proton irradiations have a negligible impact on their characteristics due to their nanoscale. However, tunnel junctions are very sensitive to nuclear radiation. The highly energetic thermal pulse accompanying nuclear radiation boosts interdiffusion, which is very severe for the tunnel junction. The strength of nanoscale junctions under high-energy particle irradiation is the weakness under nuclear radiation.

Radiation-induced order-disorder transition in InGaP

MOVPE-grown $InGaP_2$ is known for the predisposition of In and Ga to order on the group III sublattice along the <111> direction. This phenomenon is driven by the reconstruction of the surface and step motion during the MOVPE growth, depending both on the orientation of the substrate [13] and on growth parameters such as temperature, V/III ratio [14,15], and growth rate [16]. The most attractive effect associated with ordering in $InGaP_2$ is the predicted decrease of 260 meV in the band-to-band transition [17]. Therefore, ordering effects might be used to modulate the absorption limit by modifying the growth parameters, without introducing any lattice mismatch. By exploiting this behavior, the spectral response of the $InGaP_2$ top cell, and thus, the multijunction cell output, could possibly be optimized. The radiation response of the ordered $InGaP_2$ semiconductor is thus of great interest.

Figure 5a is a monochromatic CL image showing the ordered domains in the $InGaP_2$ along the [110] direction. Darker areas are possibly associated with antiphase boundaries (APBs). The CL spectra are shown in Figure 5b. A_0 is the spectrum excited on *ordered* $InGaP_2$ (o-InGaP) prior to irradiation. After doses as high as 10^{11} MeV g^{-1}, there is little effect on the spectrum (A_1). However, in *partially ordered* $InGaP_2$ (see spectrum B_0) the subsequent irradiation (spectrum B_1, $D_d \sim 10^{11}$ MeV g^{-1}) disorders the structure. We have finally confirmed the occurrence of a radiation-induced order-disorder transition in $InGaP_2$ by combining CL measurements and transmission electron microscopy observations [4].

Estimates of the lifetime damage coefficient under proton irradiation lead to 10^{-12} $gMeV^{-1}$ and 10^{-13} $gMeV^{-1}$ for disordered and ordered InGaP, respectively. Therefore, ordered structures seem to be even more radiation tolerant than partially ordered or disordered ones. A first attempt to explain these results is from the coordination of phosphorous in ordered and disordered InGaP. Within ordered domains, P is coordinated to either $InGa_3$ or In_3Ga. Disordering the structure, we find additionally P coordinated to In_4, In_2Ga_2, and Ga_4. Displacement of indium by irradiation should be preferential due to the mutual relationship between the energy of the In-P and Ga-P bonds. The displacement of an In atom in an In_2Ga_2 environment leads to $InGa_2$ that is more

electronegative and thus less stable than In_2Ga^- from In_3Ga. A statistical approach shows then that the higher the degree of ordering, the lower is the density of vacancies produced after irradiation.

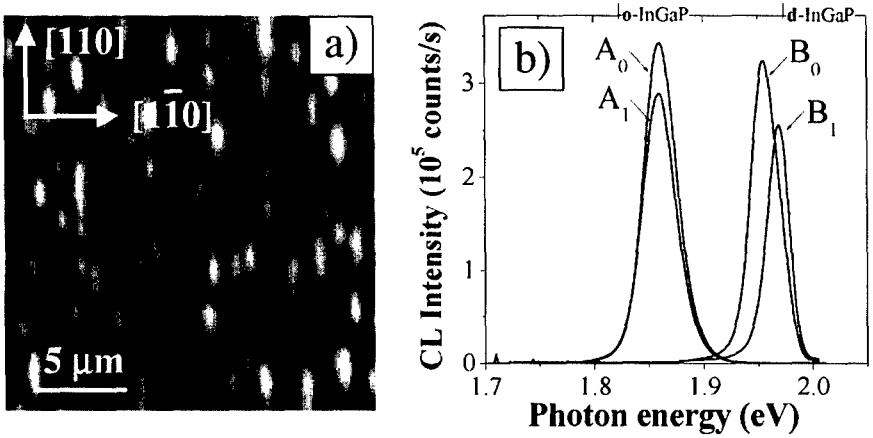

Figure 5. (a) Monochromatic CL image showing ordered domains in $InGaP_2$. (b) CL spectra of $InGaP_2$ for *ordered* InGaP (A) and *partially ordered* InGaP (B), before and after irradiation (0 and 1 subscripts, respectively).

Summary and novel schemes

The radiation response of a multijunction device is determined by the response of the most vulnerable individual sub-cell. The use of $InGaP_2$/GaAs cells in severe radiation environments is thereby limited by GaAs sub-cell. However, a multijunction device consisting of highly ordered $InGaP_2$ as a top cell and a disordered semiconductor as a bottom cell (OD $InGaP_2$) may increase the efficiency above single-junction $InGaP_2$ devices, avoid lattice mismatch, and have a much improved radiation resistance than current $InGaP_2$/GaAs technologies. In a first estimate from the damage coefficients, the same degradation of the output after one year of service of a $InGaP_2$/GaAs cell would be reached by the order-disordered heterostructure in as much as 10 to 100 years. The selection between $InGaP_2$/GaAs or OD $InGaP_2$ would be driven by the expected dose of radiation and the requirements of power density through the lifetime of the solar panel.

QUANTUM-WELL SOLAR CELLS

Another advanced solar cell made of multiple absorbers is based on quantum wells. Quantum-well solar cells show extended spectral sensitivity by absorption of lower-energy photons. However, these cells are predicted to have the same ideal efficiencies as the single-junction solar cell in the unity quantum-efficiency limit. Hot carriers must be extracted to produce either higher photovoltages or photocurrents. Higher photovoltages require carriers to be extracted before thermalization, whereas enhanced photocurrents are associated with production of additional carriers by impact ionization. In both approaches, hot-carrier relaxation rates should be considerably reduced, making the other processes competitive with thermalization. Quantization effects may dramatically reduce hot-carrier relaxation and, therefore, quantum wells might have the potential to increase the maximum conversion efficiency predicted by Shockley and Queisser. We have investigated the carrier excess dynamics and the effects of irradiation in quantum-well solar cells by beam injection techniques. These cells are InP single-junctions, in which a ten-period, strained $InAs_xP_{1-x}/InP$ multiple quantum well is incorporated between the emitter and the base.

Carrier excess dynamics in quantum-well solar cells

Improved efficiencies are anticipated by exploiting the increase of short-circuit current densities provided by incorporating quantum wells in the depletion region of a single-junction cell. Unfortunately, an increase in efficiency is frequently not achieved because of significant degradation in the open-circuit voltage (V_{OC}), as a result of carrier relaxation in quantum wells. It has been shown experimentally that a threshold built-in electric field must be exceeded for an optimum collection of carriers [3]. Figure 6 shows EBIC scans across the quantum wells for one of the $InAs_xP_{1-x}/InP$ cells, which is representative of the cells investigated. At lower excitation densities, there is no saturation in the induced current at the quantum well-region, and therefore, carrier collection is not optimized. Saturation is attained at higher excitation levels instead. By modeling the measured EBIC, we have shown that the main loss mechanism for non-optimized cells within the intrinsic region is carrier capture at the quantum wells [18]. Table II shows the measured V_{OC} for the $InAs_xP_{1-x}/InP$ structures of different well widths and arsenic contents, as well as calculations by the ideal theory of Anderson, in the unity quantum-efficiency limit with radiative recombination [19]. For shallow quantum wells, which show optimum collection, reasonable agreement is observed. For the cells with deeper wells, better agreement is seen when capture lifetimes (as determined by EBIC) are taking into account.

Table II. Measured and calculated V_{oc} for the strained $InAs_xP_{1-x}/InP$ quantum well solar cells. The measurements were made under 1 sun, AM0 solar spectrum.

ID	Well width (Å)	Arsenic content	V_{OC} (V) exp.	V_{OC} (V) ideal theo.	V_{OC} (V) w/capture lifetimes	Optimized collection
N1	18	0.37	0.73	0.74	...	yes
N2	12	0.65	0.71	0.73	...	yes
N3	12	0.66	0.70	0.73	...	yes
N4	31	0.32	0.61	0.69	0.64	no
N5	20	0.53	0.61	0.65	0.60	no

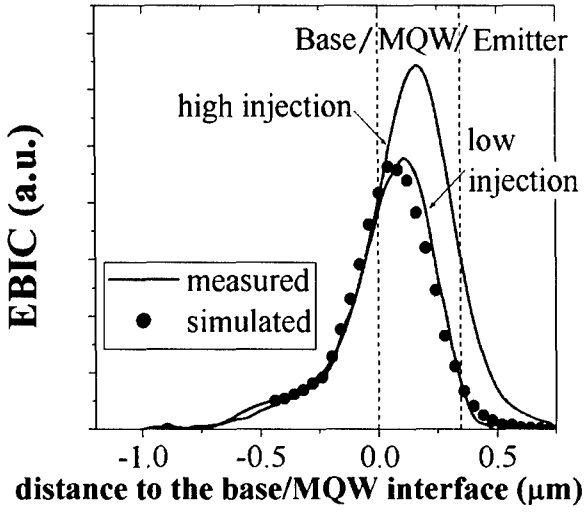

Figure 6. EBIC scans recorded under low and high excitation densities for the $InAs_xP_{1-x}/InP$ quantum-well solar cell N4.

The effect of irradiation on the operational characteristics of quantum-well solar cells can be incorporated into the ideal theory by adding the contribution of the radiation-induced defects to the nonradiative recombination lifetime. Diffusion lengths along the quantum wells were measured using the *mask method* in CL [20] before and after proton irradiation. The data suggest that solar cells with deeper quantum wells will be more sensitive to irradiation, although lifetime degradation coefficients are similar for the $InAs_xP_{1-x}$ /*InP* wells studied. Recombination of carriers through nonradiative transitions increases the rate of carrier capture by quantum wells. Carrier capture is detrimental for cell performance and should be avoided. The use of these solar cells in space is therefore limited by the relaxation of photogenerated carriers within the wells.

Interdiffusion

Energy transferred to the quantum wells under proton irradiation might result in interdiffusion by displacing As from the wells to the InP barriers. Indeed, we have observed a systematic shift of the quantum well-emission to lower photon energies (see CL spectra in Figure 6b), suggesting interdiffusion of arsenic. It is worth noting that although both N1 and N2 cells (see Table II) were designed to provide nearly identical energy states in the wells, the well thickness and As content are substantially different. Displacement of As from $InAs_xP_{1-x}$ requires less energy than that of P, and interdiffusion might be preferential for N2. Indeed, the quantum-well emission shifted up to 5 meV and 15 meV under irradiation for N1 and N2, respectively. For thinner wells such as N2, wave functions are expected to spread further into the barriers; hence, is the device rendered more sensitive to effects in the barriers and at the quantum-well/barrier interfaces.

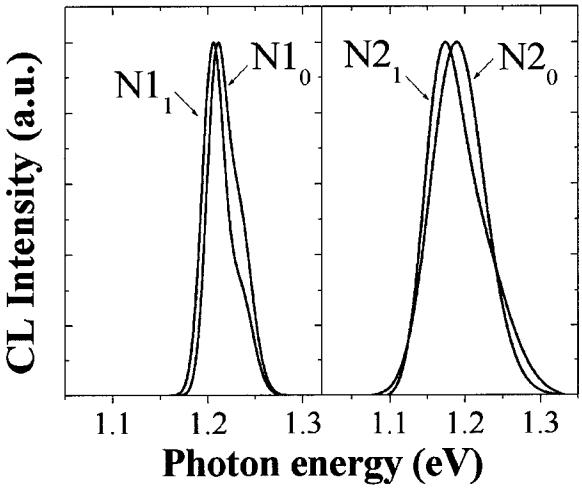

Figure 7. Effect of proton irradiation on the quantum-well luminescence for the $InAs_xP_{1-x}/InP$ structures N1 and N2 (0 and 1 subscripts correspond to before and after irradiation, respectively) .

Summary and novel schemes

Quantum-well solar cells are predicted to increase the efficiency of solar cells by using hot carriers. However, a major factor limiting the performance of these cells is the capture of photogenerated carriers. Quantization in quantum wells is restricted to the confinement direction, and the other two classical dimensions possibly govern the relaxation dynamics of the carrier excess. Indeed, the ideal theory for quantum-well solar cells, which has proven to be successful in explaining their behavior, is fundamentally classical in nature. Quantum dots are quantized in three dimensions, and the probability of reducing the loss of photocarriers by recombination in the dots is much higher. Electronic minibands formed by coupling of quantum dots may dramatically increase the diffusion of carriers across the absorber. The use of quantum dots for solar energy conversion therefore becomes an attractive approach to be explored in the future.

ACKNOWLEDGMENTS

We would like to thank A. Bett of Fraunhofer ISE and A. Freundlich of the University of Houston for providing the solar cells for irradiation testing. This work was supported by the DOE at NREL and by the U.S. Office of Naval Research at NRL.

REFERENCES

1. S.R. Kurtz, D. Myers, and J.M. Olson, "Projected performance of three- and four-junction devices using GaAs and GaInP," in *Proceedings of the 26th IEEE Photovoltaic Specialists Conference*, pp. 875-878 (1997).
2. J.M. Olson, J.F. Geisz, S.R. Kurtz, and A.G. Norman, "1-eV semiconductors for multijunction solar cells" at this conference.
3. I. Serdiukova, C. Monier, M.F. Vilela, and A. Freundlich, *Appl. Phys. Lett.* **74**, 2812 (1999).
4. M.J. Romero, D. Araujo, R. Garcia, R.J. Walters, G.P Summers, and S.R. Messenger, *Appl. Phys. Lett.* **74**, 2684 (1999).
5. A.W. Bett, R. Adelhelm, C. Agert, R. Beckert, F. Dimroth, and U. Schubert, *Solar Energy Materials and Solar Cells* **66**, 541 (2001).
6. S.I. Molina, F.J. Pacheco, D. Araujo, R. García, A. Sacedón, E.Calleja, Z. Yang, and P. Kidd, *Appl. Phys. Lett.* **65**, 2460 (1994)
7. L. Lazzarini, C. Ferrari, S. Gennari, A. Bosacchi, S. Franchi, M. Berti, A.V. Drigo, F. Romanato, and G. Salviati, *Inst. Phys. Conf. Ser.* **157**, 149 (1997)
8. The displacement damage dose (D_d) is given by the product of the particle fluence, which is expressed in cm^{-2}, and the calculated non-ionizing energy loss (NIEL, in $MeVcm^2g^{-1}$).
9. H.Y. Tada, J.R. Carter, B.E. Anspaugh, and R.G. Downing, *The Solar Cell Radiation Handbook*, JPL Publication 82-69 (1982).
10. R.J. Walters, M.J. Romero, D. Araujo, R. García, S.R. Messenger, and G.P. Summers, *J. Appl. Phys.* **86**, 3584 (1999).
11. M.J. Romero, J.M. Olson, and M.M. Al-Jassim, "Light-biasing electron-beam-induced-current for multijunction solar cells," in *Proceedings of the NCPV Program Review Meeting*, pp. 289-290 (2001).
12. C. Donolato, *Optik* **52**, 19 (1978/79).
13. K. Sinha, A. Mascharenhas, R.G. Alonso, G.S. Horner, K.A. Bertness, S.R. Kurtz, and J.M.Olson, *Solid State Communications* **89**, 843 (1994).
14. H. Murata, I.H. Ho, G.B. Stringfellow, and J.B. Mullin, *J. Crys. Growth* **170**, 219 (1997).
15. Y.S. Chun, H. Murata, G.B. Stringfellow, and J.B. Mullin, *J. Crys. Growth* **170**, 263 (1997).
16. Y.S. Chu, S.H. Lee, I.H. Ho, and G.B. Stringfellow, *J. Crys. Growth* **174**, 585 (1997).
17. S.H. Wei, and A. Zunger, *Appl. Phys. Lett.* **56**, 662 (1990).
18. R.J. Walters, G.P. Summers, S.R. Messenger, M.J. Romero, M.M. Al-Jassim, R. Garcia, D. Araujo, A. Freundlich, F. Newman, and M.F. Vilela, *J. Appl. Phys.* **90**, 2840 (2001).
19. N.G. Anderson, *J. Appl. Phys.* **78**, 1850 (1995).
20. Y. Tang, D.H. Rich, A.M. Moy, and K.Y. Cheng, *Appl. Phys. Lett.* **72**, 55 (1998).